International Journal of Heat and Mass Transfer 196 (2022) 123220

Contents lists available at ScienceDirect

International Journal of Heat and Mass Transfer

journal homepage: www.elsevier.com/locate/hmt

Measurement of interacting ethanol droplets evaporation at moderately elevated temperature and pressure using phase rainbow refractometry

Qimeng Lv, Yingchun Wu*, Xinhao Wang, Lei Zeng, Xuecheng Wu

State Key Laboratory of Clean Energy Utilization, Zhejiang University, Hangzhou 310027, China

ARTICLE INFO

Article history:
Received 22 April 2022
Revised 19 June 2022
Accepted 4 July 2022
Available online 19 July 2022

Keywords:
Droplet evaporation
Phase rainbow refractometry
Droplet interaction
Temperature
Pressure

ABSTRACT

Evaporation characteristics of interacting fuel droplets under the joint effect of ambient pressure, temperature and droplet size and spacing are critical to combustor design and simulation validation. This work reports an experimental study of evaporating monodisperse ethanol droplets at moderately elevated temperature (up to 673 K) and pressure (0.1-1.0 MPa). Evolution of droplet size and temperature along the measurement line and its evaporation rate were simultaneously measured using recently developed phase rainbow refractometry. The respective effects of the ambient conditions and droplet interactions on the heat and mass transfer of droplets were jointly studied. The results suggest that at lower ambient temperatures the droplet evaporation rate decreases with increasing ambient pressure. While at higher temperatures, the trend is reversed. Moreover, the dimensionless spacing parameter C of the droplets was well controlled to investigate the effect of inter-droplet interactions on evaporation under different ambient conditions. Strong droplet interactions, significantly inhibiting the droplet evaporation, were found to be influenced by ambient pressure. For the specific condition of droplet evaporation under low ambient temperature (373 K) and high pressure (1.0 MPa), the evaporation rate of droplets with $C = 1.85$ decreases by 19.1 % compared to droplets with $C = 3.73$. Furthermore, the correlations for Nusselt and Sherwood numbers are inferred by parametric study of the influence of the involved characteristic numbers.

1. Introduction

Design and simulation of the modern combustion chamber of liquid-fueled internal combustion devices, such as aero-engines and direct injection engines, requires an accurate understanding of heat and mass transfer of the fuel spray. The injected fuel liquid is atomized into several droplets and evaporates in the hot and pressurized gaseous medium. Then the fuel vapour burns and releases energy for propulsion.

Extensive research has been performed for simulations and experiments of the evaporation on an isolated, stagnant fuel droplet [1–3]. However, in a practical combustor, the droplet generally exists in a cluster where the heat and mass transfer are significantly dominated by the droplet interactions. Thus, the investigation of evaporation and combustion of interacting droplets is desirable. Modelling the heat and mass transfer processes involved in droplet interactions is complex and a challenge [4,5]. From an experimental point of view, studies dealing with this topic generally focused on stationary droplets supported by fibres. Mikami [6] investigated the combustion of two suspended droplets at ambient pressure up to 6 MPa under free-falling microgravity conditions. Results show that the pressure dependence of the burning rate for interacting droplets is similar to that of the isolated droplet. Wang et al. [7] studied the evaporation characteristics of three suspended droplets with equal spacing. The effect of droplet interaction significantly increases the droplet lifetime. And this influence decreases with increasing ambient temperature. However, it has been shown that the droplet suspension technique would significantly increase the droplet evaporation rate through the energy transfer from fibres to droplets [8].

Recent works have paid extensive attention to avoiding additional sources of interference by using advanced droplet generation techniques. The monodisperse droplets stream generator is a useful tool to accurately regulate droplet interactions. For a series of uniformly arranged droplets, the size, velocity, spacing and temperature of the droplets can be easily adjusted at the injection. Based on this device, numerous experimental researches have been conducted [9–11]. Generally, the droplet size variation was measured by using photographic imaging techniques. More accurate light

* Corresponding author.
E-mail address: wycgsp@zju.edu.cn (Y. Wu).

https://doi.org/10.1016/j.ijheatmasstransfer.2022.123220
0017-9310/

Nomenclature

C	dimensionless spacing parameter
D	droplet diameter
S	droplet inter spacing
P	Pressure
T	temperature
v	velocity
n	refractive index
K	evaporation rate constant
t	time
D_v	vapour diffusion coefficient
B_M	Spalding mass transfer number
Sh	Sherwood number
Y	mass fraction
Re	Reaynolds number
Sc	Schimidt number
$\dot{m}_d$	fuel vapour flow rate
m_d	droplet mass
Le	Lewis number
p	vapour pressure
G	correction factor
B_T	Spalding heat transfer number
Pr	Prandtl number
L_v	latent heat of vaporization
Nu	Nusselt number
k	thermal conductivity
η	emperical correlation defined by Eq. 11
ϕ	ripple phase shift
λ	laser wavelength
ρ	density
χ	molar fraction
Φ	energy
φ	coefficient defined by Eq. 10
inj	injected liquid initial parameter
d	droplet
exp	experimental value
v	vapour
m	gas-vapour mixture
s	droplet surface
∞	infinity
sat	saturated state
g	gas phase
amb	ambient conditions

scattering bases techniques, such as rainbow refractometry (RR) and morphology dependent resonances (MDR) [10,11], were also used to estimate the size and temperature evolutions of droplets inside a linear array. By using the two-colour laser-induced fluorescence (2cLIF) technique and forward scattering interferometry (FSI), Virepinte et al. [12,13] and Castanet et al. [14–16] extensively studied the interaction effect of monodisperse droplet streams. A dimensionless spacing parameter C, is defined as the ratio of droplet distance S and diameter D_d. The evaporation rate of droplet streams was also compared with that of the isolated droplet under identical conditions, yielding several empirical correlations η for interaction modifications. Recently, phase rainbow refractometry (PRR) was used to examine the evaporation of droplets stream [17–19], demonstrating that PRR is a promising tool for measuring droplets temperature, size, as well as size variation. Nevertheless, such works of literature on the evaporation of interacting droplets only consider droplets under atmospheric pressure conditions. The quantification of how η depends on C in a droplet stream under pressure conditions has not been well investigated.

Table 1
Values of ambient temperature t_{amb}, pressure P_{amb}, droplet velocity v_d, diameter D_d and dimensionless spacing parameter C in the experiments.

Parameter				
T_{amb} (K)	293-673			
P_{amb} (MPa)	0.1-1.0			
v_d (m/s)	3.5			
D_d (μm)	153.8	136.6	116.8	108.4
C	3.73	2.94	2.15	1.85

This study is to characterize the evaporation of the moving ethanol droplet stream under moderately elevated pressure and temperature conditions by using phase rainbow refractometry. Specifically, the time evolutions of temperature and size variation of droplets for various ambient temperatures (293-673 K) and pressures (0.1-1 MPa), as well as the spacing parameters C (1.85-3.73), are determined. The interaction effect on the droplet evaporation is quantified by comparing the experimental results with the prediction model proposed by Abramzon and Sirignano [20]. And the correction factor for both heat and mass transfer processes are calculated from the experimental data.

2. Experimental setup and procedure

2.1. Experimental setup

The experimental setup is shown schematically in Fig. 1. The experiment is performed inside a high-pressure chamber (up to 1.0 MPa) fed with pressurized nitrogen. The air flow is quietened by forcing it through a copper foam plate to avoid its destabilization to the droplet stream. The electric coil produces a high-temperature field in the chamber (up to 673 K). The gas pressure and temperature can be adjusted and measured by a manometer and K-type thermocouple array mounted on the chamber enclosure, respectively. All sensors mentioned are connected to a data logger. The chamber has an inner equivalent diameter of 110 mm and a height of 160 mm, ensuring a non-saturated condition [21]. Several quartz glass windows are mounted in the wall to provide optical access.

The tested ethanol liquid is pumped by a syringe into a tube and then forced through a small orifice. A monodisperse droplets stream is obtained by imposing a series of tiny pressure disturbances on the formed laminar jet through a piezoceramic. By varying the excitation frequency at any given injection flow rate, we can alter the droplet size D_d and their separation distance S, resulting in a variable dimensionless spacing parameter C. The injection temperature of the liquid fuel T_{inj} is 293 K. At the bottom of the chamber, the fuel liquid is collected and evacuated through a valve. In addition, the spatial velocity distribution of the gas around droplet stream is characterized using particle image velocimetry (PIV). The obtained air velocity profile shows that the air velocity is rather homogeneous with a value ranging between 0.1-0.3 m/s. The gas flow ensures an almost uniform temperature field in the chamber and also prevents vapour saturation. Ambient conditions and droplet parameters for each studied case are reported in Table 1.

A sketch of the experimental setup for the detection of droplet size, refractive index, and evaporation rate is shown in Fig. 1 (right). The 532 nm laser sheet illuminates the droplets stream, and the scattering light of droplets is recorded with the PRR apparatus 30 mm downstream of the nozzle. The high periodicity achieved with the monodisperse droplet stream allows converting the droplet moving distance into time. Thus, the diameter and temperature evolution of the droplet stream can be monitored as a function of time.

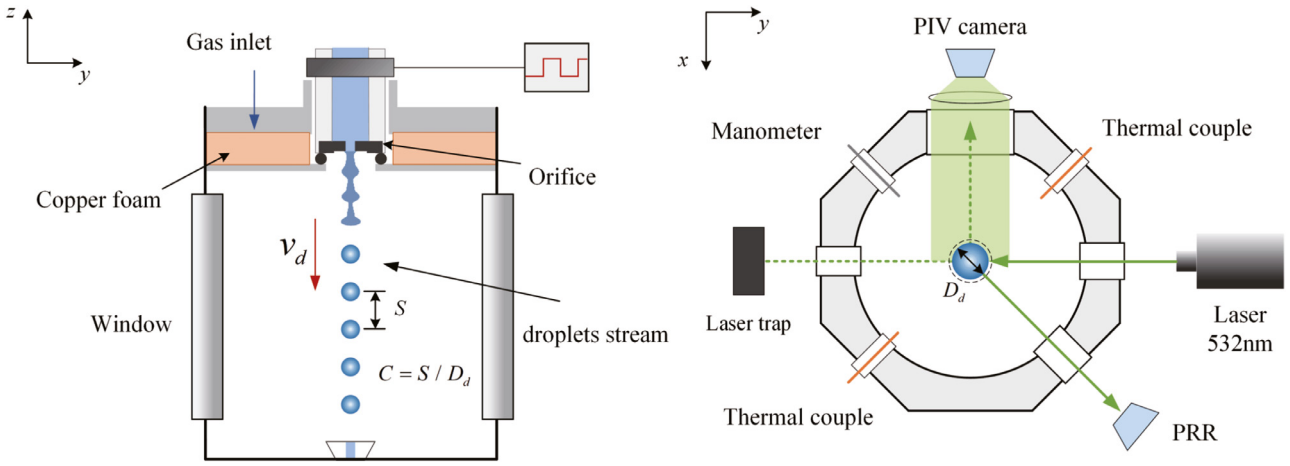

Fig. 1. Sketch of the experimental setup and the optical access for different optical techniques.

2.2. Droplet temperature, size and evaporation rate measurement

The refractive index of ethanol decreases linearly by 0.0004 for 1 K increase in temperature [22], which can be used to convert refractive index values into droplet temperature. Since the liquid inside the chamber is surrounded by high-pressure gas, we are not able to measure directly the absolute refractive index of but refractive index of droplets relative to the ambient gas. The refractive index of the ambient gas n_{gas}, as a function of wavelength, temperature, and pressure, is calculated by the Edlen correlations [23]. In the tested conditions, the refractive index of gas inside the chamber varies from 1.00002 to 1.00273. Nevertheless, the refractive index of ethanol changes with ambient pressure, and is estimated using the experimental data obtained from Kanjanasakul et al [24].

Fig. shows a representative PRR image of 117 μm ethanol droplet ejected into the chamber with an ambient temperature of 323 K. Firstly, the recorded rainbow signals are filtered to remove the ripple structures from the Airy peaks to inverse size D and refractive index n of droplets, as shown in Fig.. The Airy peaks shift towards the larger angle with height (time), indicating the decreasing temperature of droplets. After that, the ripple structure is obtained by subtracting the Airy rainbow from the rainbow signals. The phase shifts ϕ between the ripple structures under different camera rows are obtained from their cross power spectral density. Once the droplet size D, refractive index n, and phase shift ϕ are known, droplet size variation can be determined by

$$\Delta D = \Delta\phi \cdot \frac{\lambda}{2\pi} \frac{3n^2}{(8+10n^2)[(n^2-1)/3]^{1/2}}, \tag{1}$$

where λ is the laser wavelength. Subsequently, the evaporation rate constant K is expressed as

$$K_{\exp} = \frac{(D+\Delta D)^2 - D^2}{\Delta t} = \frac{2D\Delta D}{\Delta t} + o\left(\frac{\Delta D^2}{\Delta t}\right), \tag{2}$$

where Δt is the measurement time duration depended on droplet velocity and the spatial resolution of the measuring device, which is 2.5 ms in this experiment. The term $o(\Delta D^2/\Delta t)$ is negligible and thus omitted in subsequent computations. More informations can be found in our previous work [17,25]. To process the image shown in Fig., we first extract the light intensity distribution averaged over 20 pixel rows and normalise it for intensity. After fast Fourier transform (FFT), the Airy peaks is seperated from the high-frequency ripple structures and is compared to the simulated intensity distribution to search the optimal fitting. Then the droplet diameter D and refractive index n can be obtained. By subtracting the Airy peaks from the original rainbow signals, we can obtain the ripple structures at each pixel row. Then the phase shift $\Delta\phi$ of ripple structure is calculated using the cross power spectral density (CPSD). Since all the parameters in Eq. 2 are known, the evaporation rate constant K_{exp} can be deduced.

It can be seen from Eqs. 1 and 2 that the accuracy of the evaporation rate measurement is mainly affected by the phase shift $\Delta\phi$, droplet size D and refractive index n. The uncertainty of phase shift $\Delta\phi$ measurement is mainly introduced by the optical system and the inversion algorithm, which is about 2% [26]. The accuracy of the droplet size determination for PRR is within 2 μm, with a relative uncertainty of approximately 1.5%. The analysis of uncertainty in refractive index measurements is more complex as the inhomogeneity inside droplets also has great effects, in addition to the errors introduced by the experimental system and inversion algorithm. It is believed that rainbow refractometry may underestimate the actual temperature values due to the refractive index gradient within the droplet, and the measurement uncertainties are acceptable at about 10% [17,27].

3. Evaporation rate model

The Abramzon-Sirignano evaporation model (ASM) [20] is adopted to describe the heat and mass transfer progresses between the liquid and gaseous phase. The employed model, derived from Ficks law, uses the vapour concentration gradient at the droplet surface as the driving force to induce vaporization. The real gas effects and the solubility of the surrounding gas into droplets are not considered [28]. In this way, the differential equations for droplet mass is given by

$$\dot{m}_d = \pi \rho_m D_d D_{v,m} Sh_m^* \ln(1+B_M), \tag{3}$$

where ρ_m is the droplet density and D_v is the vapour diffusion coefficient. And the subscript m represents that reference values for the gas-mixture physical properties are defined by the 1/3 averaging rule [29]. The Spalding mass transfer number, B_M, is given by

$$B_M = \frac{Y_{v,s} - Y_\infty}{1 - Y_{v,s}}, \tag{4}$$

recalling that $Y_{v,s}$ and Y_∞ are the fuel vapour mass fraction at the droplet surface and at infinity. For ethanol and most hydrocarbons, the phase transformation process is faster than the vapour transport, resulting in the thermodynamic equilibrium of liquid-vapour at the droplet surface. It is thus assumed that the vapour concentration is at saturated condition. Thus the surface vapour molar fraction $\chi_{v,s}$ can be estimated using Raoult's law,

$$\chi_{v,s} = \frac{p_{v,s}}{p_{amb}} = \frac{p_{sat}}{p_{amb}}. \tag{5}$$

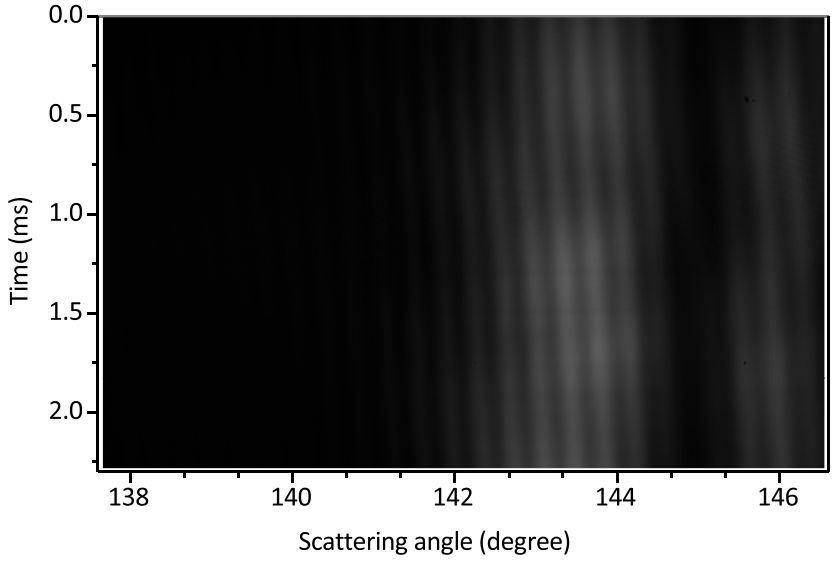

(a)

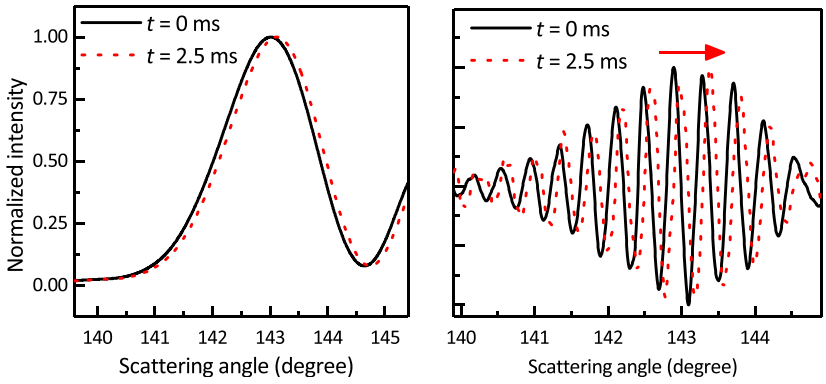

(b) (c)

Fig. 2. Rainbow image of 117 μm ethanol droplet at ambient temperature of 323 K (a). The extracted Airy rainbow signals (b) and ripple structures (c).

And the saturated vapour pressure p_{sat} is calculated by Clausius-Clapeyron equation.

Sh_m^* is the modified Sherwood number, yielding,

$$Sh_m^* = 2 + 0.6Re_d^{1/2}Sc_m^{1/3}, \tag{6}$$

where Re_d and Sc_m are the droplet Reynolds number and Schimidt number, respectively.

For small size of transparent droplets, the effects of thermal radiation is negligible, and thus the radiative heat flux is not considered. Assuming the uniform temperature inside droplet, the energy balance equation for the droplet is expressed as

$$\begin{aligned}\Phi_c &= \Phi_d - \Phi_l \\ &= G\pi D_d Nu_m^* k_m (T_g - T_d) - L_v \dot{m}_d,\end{aligned} \tag{7}$$

where Φ_d is the heat flux exchanged from gaseous phase and Φ_l is the latent energy of evaporation for vapour diffusing out. $\Phi_c = m_d c_{p,l} \cdot \mathrm{d}T_d/\mathrm{d}t$ is the sensible energy entering the droplet to increase itself temperature, where $c_{p,l}$ is the specific heat of liquid. T_g and T_d are the temperature of gaseous phase and droplet, respectively. k_m is the thermal conductivity of the gas-vapour mixture. L_v is the latent heat of vaporization and Nu_m^* is the modified Nusselt number,

$$Nu_m^* = 2 + 0.6Re_d^{1/2}Pr_m^{1/3}, \tag{8}$$

where Pr is the Prandtl number. The correction factor G is defined as $G = \ln(1 + B_T)/B_T$. B_T is the Spalding thermal energy transfer number following the relation,

$$B_T = (1 + B_M)^{\varphi} - 1, \tag{9}$$

where

$$\varphi = \left(\frac{c_{p,v}}{c_{p,g}}\right)\left(\frac{Sh_m^*}{Nu_m^*}\right)\frac{1}{Le_m}, \tag{10}$$

$Le_m = k_m/(c_{p,m}\rho_m D_m)$ is the Lewis number.

4. Results

4.1. Effects of ambient temperature and pressure

To determine the respective influence of the ambient and injection parameters, droplets generated at the same excitation frequency are selected for the following analysis. Here the droplet initial diameter is 117 μm and its spacing parameter C is 2.15. Fig. 3 shows the temporal variation of normalized droplet size square at different ambient temperatures. As the measurement started from a certain distance after jet disintegration, the droplet heat-up period is not observed in this figure. As expected, increasing the ambient temperature leads to an increase in droplet evaporation rate.

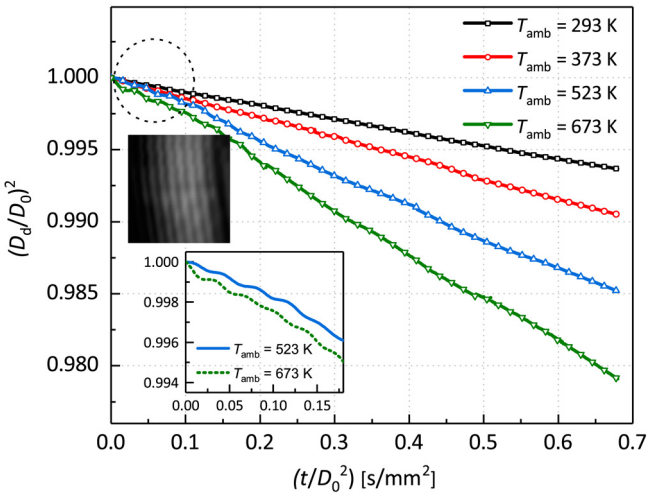

Fig. 3. Normalized squared droplet size with time for various ambient temperatures.

For instance, as the temperature is raised from 293 K to 673 K, the evaporation rate increases from 0.0093 mm^2/s to 0.0308 mm^2/s. As can be seen in Fig. 3, at the ambient temperature with 523 K and 673 K, the fluctuation of the rainbow pattern occurs in the initial measurement stage ($(t/D_0)^2 < 0.1$), which is caused by the tiny oscillation of the droplet [30]. The liquid ligaments generated after jet breakup firstly transform into oscillating droplets under the action of surface tension. And the oscillation amplitude decays due to the viscosity, leading to the droplet at an equilibrium state. When the ambient temperature rises, droplets are heated by the surrounding gas, resulting in an increase in droplet temperature and a decrease in its viscosity. Therefore, the droplet oscillation is not dissipated completely by the viscosity during this period and leads to the fluctuation of rainbow patterns. The phase shift induced by droplet oscillation is superimposed on the phase shift caused by evaporation. This phenomenon has a negligible effect on the measurement of evaporation rate, as it is determined by a linear fit.

Previous numerical and experimental investigations [4,31] show that the gaseous temperature affects the way the droplet evaporation rate varies with ambient pressure. Therefore, the gas temperature should be considered when analyzing the droplet evaporation characteristics at various ambient pressure. Fig. 4 shows the temporal evolution of the experimentally obtained droplet normalized size and temperature. Noted that due to the non-negligible aerodynamic effects arising at higher ambient temperature, the liquid irregularities disrupt the jet surface, resulting in the jet disintegration in the second wind-induced breakup regime [32]. At T_{amb} = 293 K and p_{amb} = 1.0 MPa, the generated droplets are not uniform and smaller than the jet diameter, and hence not shown. In the cases of ambient temperatures of 273 and 373 K, the droplet heating is almost completely compensated by the evaporation cooling effect.In Fig. and Fig. 4d at higher ambient temperatures, more heat is transferred to the interior of the droplet and the initial droplet temperature increases. Additionally, the droplet temperature reaches higher values at higher ambient pressure, because the evaporation of the droplet is hindered and less heat is lost for evaporation.

Over 100 rainbow images were recorded and processed under each experimental condition to ensure the reliability of the experiment. By calculating the slope of droplet size history, the evaporation rate constant K_{exp} can be obtained and is presented in Fig. 5 for each case. And the relative errors for evaporation rate constant are within 10%. It can be seen that the droplet evaporation rate decreases with the ambient pressure at lower gas temperature (Fig. and), but increase at higher gas (Fig. and 4 d). This trend is attributed to the phase equilibrium between the vapour at the droplet surface and surrounding gas. At lower ambient temperature, increasing the ambient pressure decreases the vapour mass fraction at droplet surface ($p_{v,s}$), thus reducing the evaporation rate (Eq. 5). However, once the droplet surface temperature reaches a certain value where the increased rate of saturated vapour pressure promotes the evaporation rate more than the inhibition effect of the increase in ambient pressure, as demonstrated by Eq. 4, exacerbating the evaporation rate. This suggests the existence of a threshold ambient temperature which determines whether the ambient pressure would enlarge or reduce the droplet evaporation rate.

4.2. Effects of droplet interaction

As mentioned before, the effect of interaction between droplets has been numerically and experimentally studied [13,16], deriving several C dependent corrective factors. In this experiment, the spacing parameter C is modified by changing the excitation frequency of the piezoelectric ceramics. The joint effects of ambient temperature and pressure together with the interaction of droplets are investigated in this section.

Fig. 6 shows the experimental evaporation rate constant K_{exp} for the ambient temperature of 373 and 673 K, pressure from 0.1 to 1 MPa, and droplet dimensionless spacing parameters from 1.85 to 3.73. As expected, increasing the spacing parameter C causes an augmentation of droplet evaporation rate for all cases. As an example for ambient pressure at 0.1 MPa, decreasing the spacing parameter from 3.73 to 1.85 at 373 K Fig. 6a) reduces the droplet evaporation rate by 19.1%, and at 673 K (Fig. 6b) this value is 18.7%. Actually, decreasing the droplet relative spacing increases the ambient fuel vapour concentration (Y_∞), resulting in a decrease in the Spalding number B_M (Eqs. 4 and (5) and consequently, the reduction of mass diffusion. It also indicates that this tendency of droplet interaction affecting evaporation is almost independent of the ambient temperature at atmospheric pressure. Results of droplet temperature indicate that the energy transfer from the ambient gas to droplet is insensitive to the spacing parameter, which is consistent with conclusion obtained by Lavieille [33] et al.

It can be seen from Fig. 6 that the way ambient pressure changes droplet interactions on evaporation varies at different temperatures. At lower ambient temperature (373 K), as presented in Fig. 6a, for P_{amb} = 0.1 MPa, the increase of droplet evaporation as expanding droplet spacing from C = 1.85 to 3.73 is 19.1%, while for 1.0 MPa the value is 11.3%. In contrast, as the ambient temperature increases to 673 K, shown in Fig. 6b, the effect of interactions on evaporation is almost identical at different pressures. Therefore, it can be concluded that the effect of droplet interaction is prominent for higher ambient pressure at lower ambient temperature. In the following, the underlying mechanism will be identified by the competitive effects of mass and heat transfer on droplet evaporation.

To include the influence of droplet interactions, Castanet et al. [16] introduced the reduction factors η_T and η_M as

$$\eta_T = Nu_{exp}/Nu_{iso} \quad \text{and} \quad \eta_M = Sh_{exp}/Sh_{iso}, \tag{11}$$

where Nu_{exp} and Sh_{iso} are derived using Eq. 8 and 6. Furthermore, based on the assumption of unitary Lewis number, η_T is equal to η_M, indicating the similarity between the heat and mass transfer.

The experimental Sherwood and Nusselt number are calculated from the temperature history and evaporation rate of the droplet stream,

$$Sh_{exp} = \frac{3K_{exp}}{2D_{v,m}\ln(1+B_M)}. \tag{12}$$

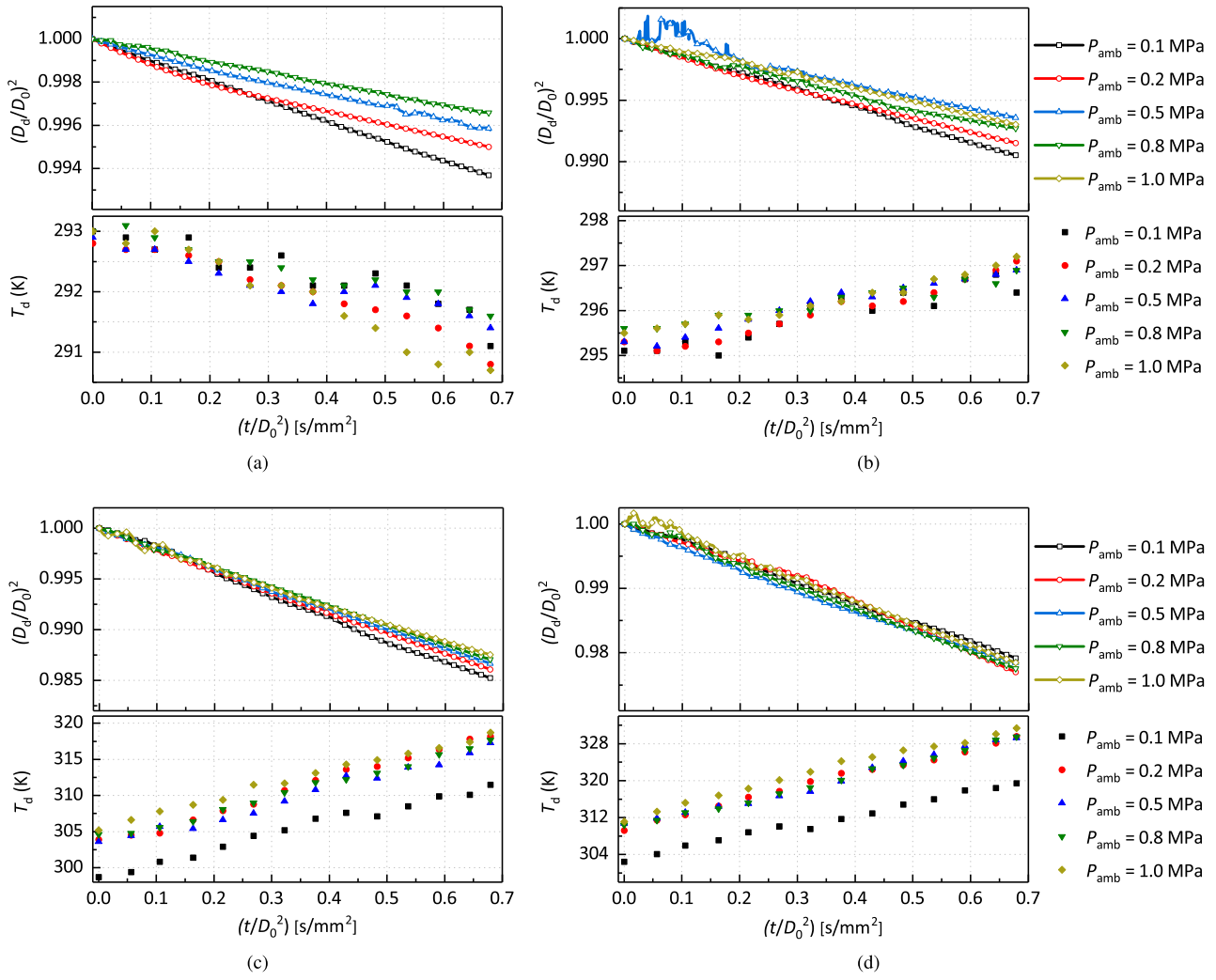

Fig. 4. Variation of normalized squared droplet diameter under different ambient conditions: 4 a 293 K, 4 b 373 K, 4 c 523 K and 4 a 673 K.

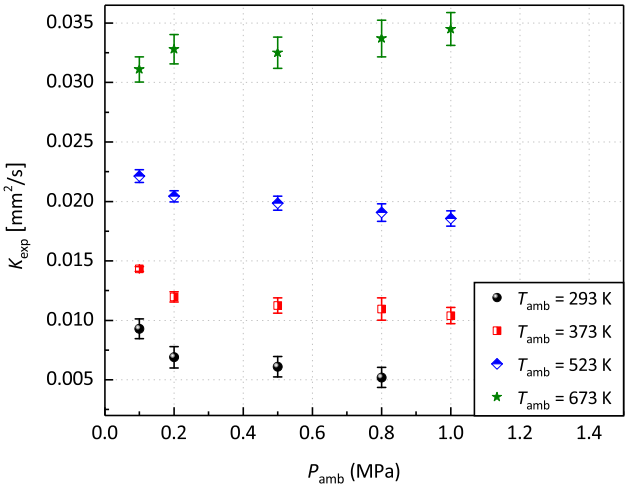

Fig. 5. Droplet evaporation constants K_{exp} at various ambient temperatures and pressures.

and

$$Nu_{exp} = \frac{\rho_m}{12Gk_m}\frac{2D_d c_{p,m} dT_d/dt - 3L_v K_{exp}}{T_{amb} - T_d}. \quad (13)$$

Since all the parameters on the right side of Eqs. 12 and 13 are either known a priori (gaseous mixture properties) or can be deduced (T_d, K_{exp} and dT_d/dt), the values of η_M and η_T can be calculated directly from the experimental results. Meanwhile, the physical properties of the liquid and gas phases can be considered as constants due to the small change in temperature. Noted again that the measurement may underestimate the value of dT_d/dt and, consequently, η_T. The calculated values of η_M and η_T are shown in Fig. 7. As expected, the interaction parameters for both heat and mass transfer increase with the dimensionless spacing parameters C. Castanet et al. [34] suggested the following formulation of the droplet interaction phenomena,

$$\frac{Nu_{exp}}{Nu_{iso}} = \frac{Sh_{exp}}{Sh_{iso}} = \eta(C). \quad (14)$$

For P_{amb} = 0.1 MPa, this formula is approximately valid. And the obtained value of $\eta(C)$ is compared with the correlation proposed by Virepinte et al. [12], which is expressed as

$$\eta(C) = 0.58 - 0.42\left[\frac{\exp[-0.19\cdot(C-5)] - \exp[0.6\cdot(C-5)]}{\exp[-0.19\cdot(C-5)] + \exp[0.6\cdot(C-5)]}\right]. \quad (15)$$

Fig. 8 summarized the values of $\eta(C)$ at P_{amb} = 0.1 MPa from Fig. 7 and the regression curve calculated by Eq. 15 which yields a regression coefficient of R^2 = 0.9835. However, Eq. 14 is limited

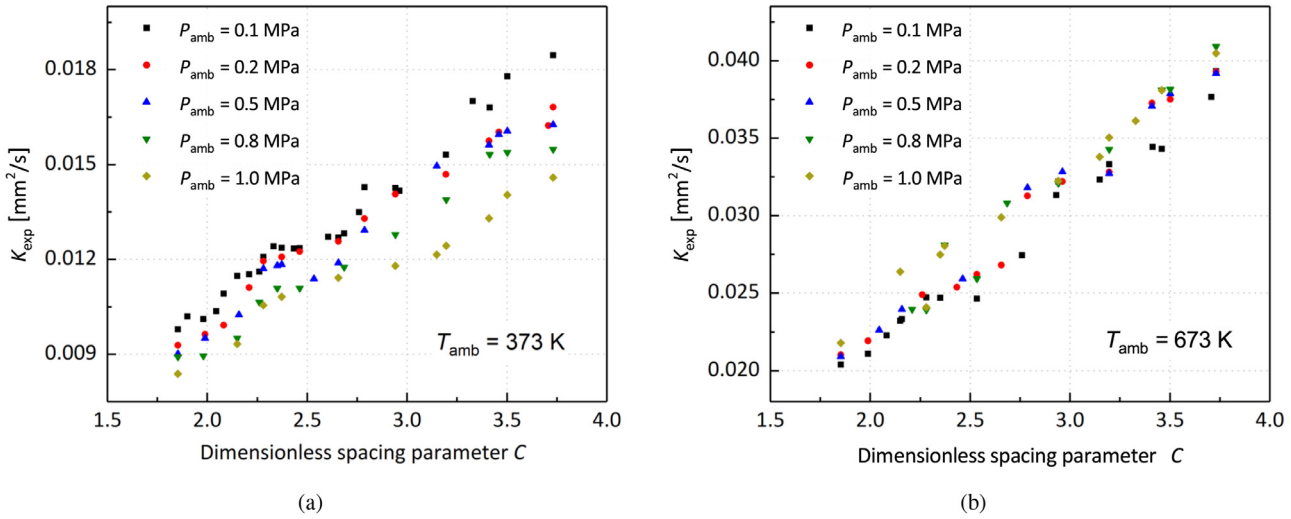

Fig. 6. Experimental evaporation rate constant K_{exp} under different ambient conditions and spacing parameters.

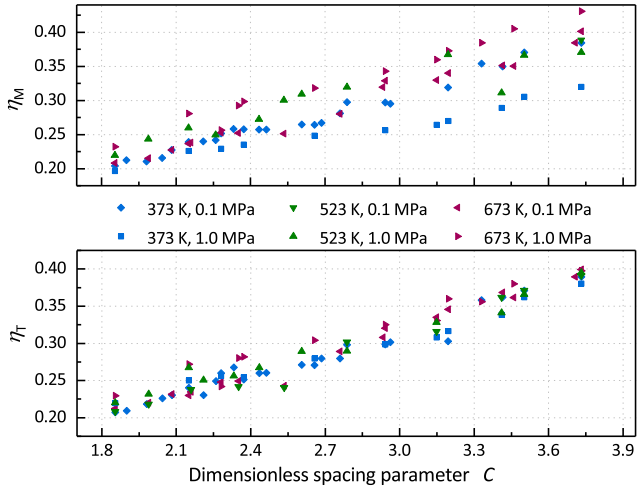

Fig. 7. The value of η_M and η_T as a function of dimensionless spacing parameter C for various experimental cases.

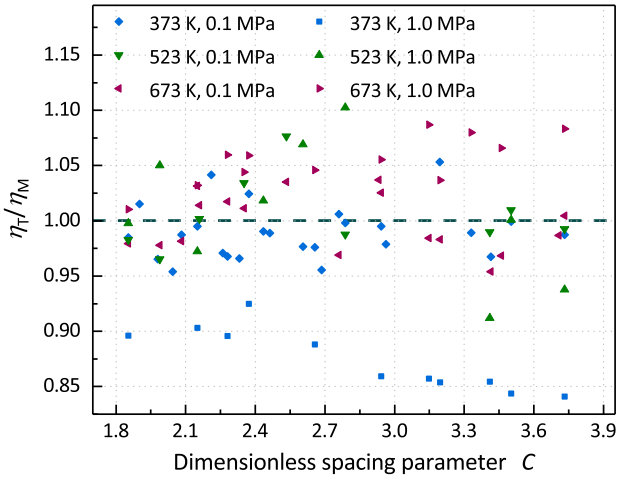

Fig. 9. Ratio of mass and heat reduction coefficient (η_M/η_T) for various experimental cases.

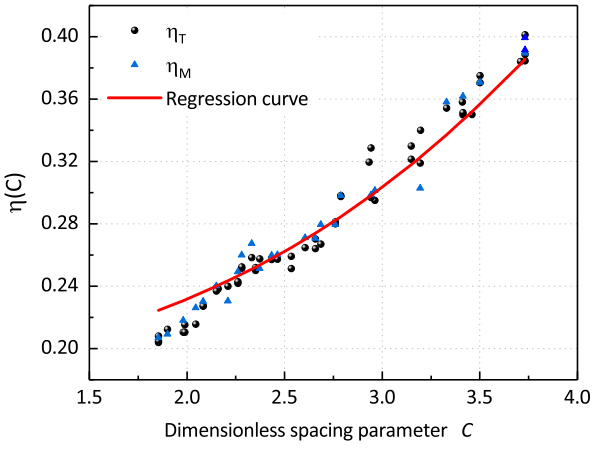

Fig. 8. Summarized evaporation rate ratio $\eta(C)$ at P_{amb} = 0.1 MPa from Fig. 7 and the regression curve.

to the cases of droplet evaporation at atmospheric pressure. The comparison of the values of η_M and η_T in Fig. 7 highlights that Nu_{exp}/Nu_{iso} and Sh_{exp}/Sh_{iso} can have completely different values at higher ambient pressure. For the cases T_{amb} = 373 K, the values of η_M at 1 MPa are significantly lower than for the ones in case 0.1 MPa. And the difference is as high as 20% for the dimensionless spacing parameter C = 3.73. The values of η_T, however, remain almost identical. Besides, for the case 673 K, the values of η_T at 1 MPa are slightly higher on average by 9% compared to atmospheric conditions.

To quantify this difference, we define the ratio of the mass and heat reduction coefficient (η_M/η_T), as presented in Fig. 9. The results of experiments conducted at atmospheric pressure (0.1 MPa) essentially satisfy $\eta_M = \eta_T$ for both temperature conditions, which is consistent with the above description. Under pressurised conditions, however, this relationship no longer holds. At lower ambient temperature (373 K), the ratio η_T/η_M reaches around 0.85, while at higher temperature (673 K) the value is around 1.10. This is because the vapour diffusion followed Fick's law and temperature followed Fourier's law are not equivalent in the present condition due to non-unity Lewis number. At lower ambient temperature, the pressure further reduces the vapour mass fraction

on the droplet surface, thus reducing the Spalding number B_M and enhancing droplet interactions on evaporation. Whereas the temperature is higher, the pressure promotes the heat transfer from the surrounding gas to the droplet, increasing the Spalding heat transfer number B_T and thus weakening the effect of droplet interaction. This suggests that the way ambient pressure affecting the interaction between droplets depends on the ambient temperature.

5. Conclusions

In this study, the effects of ambient temperature (293-673 K), pressure (0.1-1 MPa), as well as droplet interaction, on the evaporation behaviour of ethanol droplet stream are investigated. The time revolution of droplet temperature and size variation are simultaneously determined using phase rainbow refractometry.

At first, the effects of ambient temperatures and pressures on droplet evaporation were quantitatively examined. Since the effects of inter-droplet interactions are inherently present in this experiment, the droplets generated under the same excitation frequency are arranged to be analysed, ensuring that no additional effects of droplet interactions were introduced. The behaviour of droplet vaporization characterized in this work is consistent with [1,31] in the presence of temperature and pressure variations. In the present work, we mainly focus on the identification of the way droplet interaction affects evaporation for various ambient conditions.

The impact of the strong interaction is examined by the dimensionless spacing parameter C in the range of 1.85-3.73 under various ambient conditions. The interaction parameters η for both heat and mass transfer were directly estimated from the experimental obtained instantaneous droplet temperature and evaporation rate. The results suggest that, the evaporation rate of droplets decreases with the decreasing dimensionless spacing between droplets in all the ranges investigated. The values of the interaction parameters for heat and mass transfer, however, were not identical at the certain dimensionless spacing parameter, and the difference is influenced by the ambient conditions. At lower ambient temperatures, the pressure enhances the droplet-droplet interaction by further reducing the Spalding mass transfer number. And at higher ambient temperatures, pressure slightly diminishes the droplet interaction by increasing the Spalding heat transfer number. The interaction parameters η of heat and mass transfer were estimated directly from the experimentally obtained instantaneous droplet temperatures and evaporation rates. It is believed that the competition between heat and mass transfer changes the way ambient conditions affect droplet interaction.

The unitary Lewis number (Le), considering that the mass and heat diffusivity are equal near the droplet surface, is widely used as an assumption in the heat and mass transfer analysis of fuel droplets. For specific cases in this study, however, the experimentally estimated Lewis number varies approximately from 0.85 to 1.10. Therefore, for the practical combustor involving dense spray under high temperature and pressure, the assumption of unity Lewis number may not be correct. The experimental results may provide a viable data source for the modelling of the evaporation of interacting droplets under the effect of ambient conditions and potentially provide some insights for optimizing the spray in practical energy applications.

Declaration of Competing Interest

The authors declare that they have no known competing financial interests or personal relationships that could have appeared to influence the work reported in this paper.

CRediT authorship contribution statement

Qimeng Lv: Resources, Data curation, Writing – original draft. **Yingchun Wu:** Methodology, Writing – review & editing. **Xinhao Wang:** Data curation. **Lei Zeng:** Data curation. **Xuecheng Wu:** Conceptualization.

Data Availability

Data will be made available on request.

Acknowledgment

The authors gratefully acknowledge the support from project supported by National Natural Science Foundation of China (52006193, 91741129), Innovative Research Groups of the National Natural Science Foundation of China (51621005), National Science and Technology Major Project (2017-V-0016-0069), National Key Research and Development Program of China (2020YFA0405700, 2020YFB0606200). Furthermore, the authors would like to acknowledge Can Li from Nanjing University of Science and Technology (Nanjing, China) for fruitful discussions.

References

[1] H. Nomura, Y. Ujiie, H.J. Rath, J. Sato, M. Kono, Experimental study on high--pressure droplet evaporation using microgravity conditions, Symposium (International) on Combustion 26 (1) (1996) 1267–1273.
[2] S.S. Sazhin, M. Al Qubeissi, R. Kolodnytska, A. Elwardany, R. Nasiri, M. Heikal, Modelling of biodiesel fuel droplet heating and evaporation, Fuel 115 (2014) 559–572.
[3] S.S. Sazhin, Modelling of fuel droplet heating and evaporation: Recent results and unsolved problems, Fuel 196 (2017) 69–101.
[4] T. Kitano, J. Nishio, R. Kurose, S. Komori, Effects of ambient pressure, gas temperature and combustion reaction on droplet evaporation, Combust. Flame 161 (2) (2014) 551–564.
[5] B. Wang, A. Kronenburg, G.L. Tufano, O.T. Stein, Fully resolved dns of droplet array combustion in turbulent convective flows and modelling for mixing fields in inter-droplet space, Combust. Flame 189 (2018) 347–366.
[6] M. Mikami, M. Kono, J. Sato, D.L. Dietrich, Interactive effects in two-droplet combustion of miscible binary fuels at high pressure, Symposium (International) on Combustion 27 (2) (1998) 2643–2649.
[7] J. Wang, X. Huang, X. Qiao, D. Ju, C. Sun, Experimental study on evaporation characteristics of single and multiple fuel droplets, J. Energy Inst. 93 (4) (2020) 1473–1480.
[8] C. Chauveau, M. Birouk, F. Halter, I. Gökalp, An analysis of the droplet support fiber effect on the evaporation process, Int. J. Heat Mass Transf. 128 (2019) 885–891.
[9] J. Sangiovanni, A. Kesten, Effect of droplet interaction on ignition in monodispersed droplet streams, Sympos. (International) Combust. 16 (1) (1977) 577–592.
[10] G. Chen, M.M. Mazumder, R.K. Chang, J.C. Swindal, W.P. Acker, Laser diagnostics for droplet characterization: application of morphology dependent resonances, Progr. Energy Combust. Sci. 22 (2) (1996) 163–188.
[11] V. Devarakonda, A.K. Ray, Effect of inter-particle interactions on evaporation of droplets in a linear array, J. Aerosol Sci. 34 (7) (2003) 837–857.
[12] J. Virepinte, Y. Biscos, G. Lavergne, P. Magre, G. Collin, A rectilinear droplet stream in combustion: droplet and gas phase properties, Combust. Sci. Technol. 150 (1-6) (2000) 143–159.
[13] P. Lavieille, F. Lemoine, G. Lavergne, J. Virepinte, M. Lebouché, Temperature measurements on droplets in monodisperse stream using laser-induced fluorescence, Experiment. Fluid. 29 (5) (2000) 429–437.
[14] G. Castanet, P. Lavieille, F. Lemoine, M. Lebouché, A. Atthasit, Y. Biscos, G. Lavergne, Energetic budget on an evaporating monodisperse droplet stream using combined optical methods: Evaluation of the convective heat transfer, Int. J. Heat Mass Transf. 45 (25) (2002) 5053–5067.
[15] C. Maqua, G. Castanet, F. Grisch, F. Lemoine, T. Kristyadi, S. Sazhin, Monodisperse droplet heating and evaporation: experimental study and modelling, Int. J. Heat Mass Transf. 51 (15-16) (2008) 3932–3945.
[16] G. Castanet, L. Perrin, O. Caballina, F. Lemoine, Evaporation of closely-spaced interacting droplets arranged in a single row, Int. J. Heat Mass Transf. 93 (2016) 788–802.
[17] Y. Wu, H. Li, X. Wu, G. Gréhan, L. Mädler, C. Crua, Change of evaporation rate of single monocomponent droplet with temperature using time-resolved phase rainbow refractometry, Proc. Combust. Inst. 37 (3) (2019) 3211–3218.
[18] C. Li, Q. Lv, Y. Wu, X. Wu, C. Tropea, Measurement of transient evaporation of an ethanol droplet stream with phase rainbow refractometry and high-speed microscopic shadowgraphy, Int. J. Heat Mass Transf. 146 (2020) 118843.

[19] Q. Lv, C. Li, Y. Wu, X. Wang, X. Wu, Effect of aluminum nanoparticles addition on the evaporation of a monodisperse ethanol droplet stream, Int. J. Heat Mass Transf. (2021) 122275.
[20] B. Abramzon, W.A. Sirignano, Droplet vaporization model for spray combustion calculations, Int. J. Heat Mass Transf. 32 (9) (1989) 1605–1618.
[21] T. Kristyadi, V. Deprédurand, G. Castanet, F. Lemoine, S.S. Sazhin, A. Elwardany, E. Sazhina, M. Heikal, Monodisperse monocomponent fuel droplet heating and evaporation, Fuel 89 (12) (2010) 3995–4001.
[22] W.M. Haynes, CRC handbook of chemistry and physics, CRC press, 2014.
[23] B. Edlén, The refractive index of air, Metrologia 2 (2) (1966) 71.
[24] C. Kanjanasakul, F. Grisch, S. Saengkaew, G. Gréhan, Optical characterization of ethane droplets in the vicinity of critical pressure, Oil Gas Sci. Technol.–Revue dIFP Energies nouvelles 75 (2020) 59.
[25] Y. Wu, J. Promvongsa, S. Saengkaew, X. Wu, J. Chen, G. Gréhan, Phase rainbow refractometry for accurate droplet variation characterization, Opt. Lett. 41 (20) (2016) 4672–4675.
[26] M. Luo, Y. Wu, O.J. Haidn, Temperature and size measurements of cryogenic spray droplets with global rainbow refractometry, J. Propuls. Power 35 (2) (2019) 359–368.
[27] P. Massoli, Rainbow refractometry applied to radially inhomogeneous spheres: the critical case of evaporating droplets, Appl. Opt. 37 (15) (1998) 3227–3235.
[28] J. Stengele, H.-J. Bauer, S. Wittig, Numerical study of bicomponent droplet vaporization in a high pressure environment, volume 78743, American Society of Mechanical Engineers, 1996.
[29] M. Yuen, L.W. CHEN, On drag of evaporating liquid droplets, Combust. Sci. Technol. 14 (1976).
[30] Q. Lv, Y. Wu, C. Li, X. Wu, L. Chen, K. Cen, Surface tension and viscosity measurement of oscillating droplet using rainbow refractometry, Opt. Lett. 45 (24) (2020) 6687–6690.
[31] A.P. Pinheiro, J.M. Vedovoto, A. da Silveira Neto, B.G. van Wachem, Ethanol droplet evaporation: Effects of ambient temperature, pressure and fuel vapor concentration, Int. J. Heat Mass Transf. 143 (2019) 118472.
[32] M. Birouk, N. Lekic, Liquid jet breakup in quiescent atmosphere: A review, Atomizat. Sprays 19 (6) (2009).
[33] P. Lavieille, F. Lemoine, M. Lebouché, Investigation on temperature of evaporating droplets in linear stream using two-color laser-induced fluorescence, Combust. Sci. Technol. 174 (4) (2002) 117–142.
[34] G. Castanet, M. Lebouché, F. Lemoine, Heat and mass transfer of combusting monodisperse droplets in a linear stream, Int. J. Heat Mass Transf. 48 (16) (2005) 3261–3275.